Observation of ice-like water layers at an aqueous protein surface

Konrad Meister[a,1], Simona Strazdaite[a], Arthur L. DeVries[b], Stephan Lotze[a], Luuk L. C. Olijve[c], Ilja K. Voets[c], and Huib J. Bakker[a]

[a]Foundation for Fundamental Research on Matter Institute for Atomic and Molecular Physics, 1098 XG Amsterdam, The Netherlands; [b]Department of Animal Biology, University of Illinois at Urbana–Champaign, Urbana, IL 61801; and [c]Department of Chemical Engineering and Chemistry and Institute for Complex Molecular Systems, Eindhoven University of Technology, 5600 MB Eindhoven, The Netherlands

Edited by Michael L. Klein, Temple University, Philadelphia, PA, and approved November 13, 2014 (received for review July 25, 2014)

We study the properties of water at the surface of an antifreeze protein with femtosecond surface sum frequency generation spectroscopy. We find clear evidence for the presence of ice-like water layers at the ice-binding site of the protein in aqueous solution at temperatures above the freezing point. Decreasing the temperature to the biological working temperature of the protein (0 °C to −2 °C) increases the amount of ice-like water, while a single point mutation in the ice-binding site is observed to completely disrupt the ice-like character and to eliminate antifreeze activity. Our observations indicate that not the protein itself but ordered ice-like water layers are responsible for the recognition and binding to ice.

antifreeze proteins | sum frequency generation | protein hydration

It is increasingly recognized that the conformational dynamics and the functioning of proteins are closely connected to the structure and dynamics of the surrounding water (1, 2). The idea of water being not just a passive spectator but an active player in dynamical processes in biosystems has gained ground both in experiment and theory (1–3). Especially, hydrophobic hydration is considered to play a key role in biological processes, ranging from protein folding to ligand binding (2, 4, 5). In the field of protein–solvent interactions, antifreeze proteins (AFPs) play an extraordinary role. These proteins must specifically recognize and bind nascent ice crystals within the vast excess of 55 M liquid water, and thus must be very sensitive to the structural differences between the two water phases. Despite this difficult molecular recognition problem, the success of AFPs as efficient protection against freezing is illustrated by a wide distribution of AFPs among psychrophilic organisms, such as insects, fish, plants, and bacteria living in freezing habitats (6–8). Each of these groups contains AFPs that have different evolutionary origins and a great diversity in structure. All AFPs are believed to function via an adsorption–inhibition mechanism in which the proteins adsorb to the surface of ice crystals and prevent their macroscopic growth (9). The ice recognition is performed at a specific side of the protein, known as the ice-binding site (IBS), which tends to be relatively flat and hydrophobic. The present work focuses on vibrational sum frequency generation spectroscopy (VSFG) of the AFP type three (AFP-III) from an Antarctic eelpout. AFP-III has been the subject of numerous experimental (10–13) and computational studies (14, 15), and these studies have identified the protein region that is responsible for the recognition of and interaction with the primary prism planes of ice, as shown in Fig. 1, *Inset*. The IBS of this globular protein of ∼7 kDa consists of a flat, relatively hydrophobic area where certain amino acid side chains are fixed in position and are believed to organize water molecules into a specific ice-like manner (11). Among those are the hydrophobic Gln9, Leu10, Ile13, Ala16, Leu19, Val20, Met21, Val51, and Gln44 as well as the hydrophilic Asn14, Thr15, and Thr18 (see Fig. S1) (10). The surface of liquids and solids can be probed with high selectivity with VSFG. In this technique, an infrared light pulse and a visible pulse are combined at the surface to generate light at their sum frequency. The generation is enhanced in case the infrared light is resonant with a molecular vibration at the surface. The technique is bulk forbidden due to symmetry, and thus highly surface specific. VSFG has been used to investigate the structure of interfacial water at various interfaces, including protein monolayers and organic molecules (16–19). AFP-III shows a strong propensity to localize at the hydrophobic water–air interface (20), thus offering the unique opportunity to study the properties of AFP-III's hydrophobic IBS with vibrational sum frequency generation (VSFG).

Results

Fig. 1 shows the VSFG spectrum of the interface of pure water and air and of an aqueous AFP-III solution at room temperature (20 °C). The spectrum of the water–air interface shows two broadbands at 3,200 cm^{-1} and 3,450 cm^{-1}, both corresponding to hydrogen-bonded OH groups. The spectrum also contains a sharp 'free OH' peak at 3,700 cm^{-1}. The double-peak shape of the hydrogen-bonded region has been explained in terms of two different types of liquid water: strongly hydrogen-bonded tetrahedrally coordinated (ice-like) water and less coordinated (water-like) water (21), a Fermi resonance with the overtone of the bending (22), and as a result of intermolecular couplings (23). The VSFG spectrum for the AFP is very different, in that instead of a broad double-peaked response, a strong, relatively narrow peak centered at 3,200 cm^{-1} is observed. The spectrum also shows two narrow peaks at 2,880 cm^{-1} and 2,950 cm^{-1} that are assigned to the methylene and methyl vibrations of the amino acid residues of the protein. The VSFG spectrum shows a dip at 2,970 cm^{-1}, which we assign to destructive interference between

Significance

Antifreeze proteins (AFPs) enable the survival of various organisms in freezing or subfreezing habitats by preventing the macroscopic growth of ice crystals. Understanding how AFPs recognize and bind ice crystals is the most important step to unravel their working mechanism. Using surface-specific sum frequency generation spectroscopy, we were able to directly probe the ice-binding site of the protein and discovered that, already at room temperature and in an aqueous solution, the antifreeze proteins arrange water molecules into an ice-like array, which they then use to bind to ice crystals.

Author contributions: K.M., A.L.D., and H.J.B. designed research; K.M., S.S., S.L., and L.L.C.O. performed research; A.L.D., L.L.C.O., and I.K.V. contributed new reagents/analytic tools; K.M. and L.L.C.O. analyzed data; and K.M., A.L.D., I.K.V., and H.J.B. wrote the paper.

The authors declare no conflict of interest.

This article is a PNAS Direct Submission.

[1]To whom correspondence should be addressed. Email: K.Meister@amolf.nl.

This article contains supporting information online at www.pnas.org/lookup/suppl/doi:10.1073/pnas.1414188111/-/DCSupplemental.

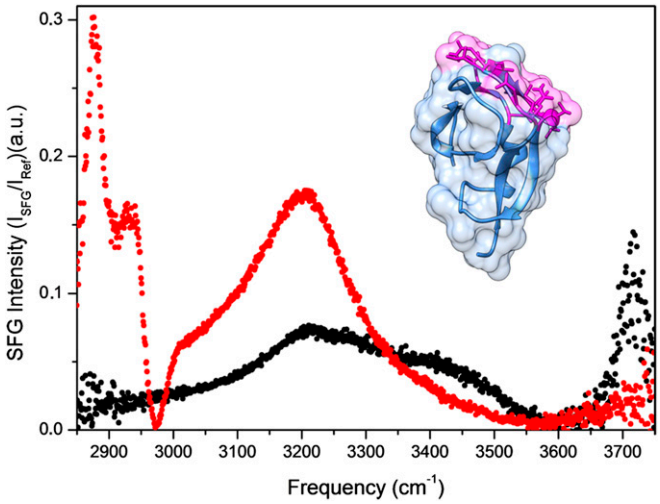

Fig. 1. VSFG spectra of the water–air interface and an aqueous solution of a 93-μM aqueous AFP-III (pH 7.8) at room temperature. The VSFG spectrum of the water–air interface (black) consists of two broadbands at 3,200 cm^{-1} and 3,450 cm^{-1} assigned to hydrogen-bonded liquid water and a sharp peak at 3,700 cm^{-1} assigned to dangling OH groups sticking out of the surface. The VSFG spectra of AFP-III (red) shows a single strong relatively narrow peak at 3,200 cm^{-1} and spectral features associated with the CH vibrations of the protein at frequencies <3,000 cm^{-1}. *Inset* shows the 3D structure of AFP-III (1MSI) with the ice-binding surface highlighted in magenta.

the response of the methyl vibrations and the low-frequency wing of the strong OH band.

Fig. 2 shows the VSFG spectra of aqueous AFP-III solutions at different concentrations at room temperature. The intensity of the 2,880 cm^{-1} and 2,950 cm^{-1} bands associated with the methylene and methyl vibration peaks rises gradually with increasing AFP-III concentration, and thus these bands form a good measure of the surface concentration of AFP-III. The response of the OH stretch vibrations strongly changes both in amplitude and shape as a function of the AFP-III concentration. At concentrations below 10 μM, the VSFG spectra show a broadband response in the frequency region of the OH stretch vibrations that is similar to the spectrum observed for the water–air interface and for solutions of other proteins. We assign the bands at ∼3,300 cm^{-1} and ∼3,400 cm^{-1} to water OH vibrations at the interface of bulk water and air. At low AFP-III concentrations, the VSFG spectrum is a sum of the spectrum of water adsorbed to AFP-III and the water–air spectrum. The amplitude of the spectrum is somewhat higher than for the pure water–air interface, which can be explained by the interfacial electric field created by proteins near the surface. We observe a similar effect for other (nonantifreeze) proteins (Fig. S2). In addition to the two broadbands, a feature at 3,600 cm^{-1} appears that we assign to water molecules that are weakly hydrogen-bonded to the protein. For AFP-III concentrations >10 μM, the broadband response at frequencies >3,400 cm^{-1} decreases with increasing AFP-III concentration and the single narrow OH peak at 3,200 cm^{-1} rises. At these higher concentrations, above the critical concentration of 10 μM, contributions from the water–air spectrum are no longer observable because of the coverage of the surface with AFP-III. The VSFG spectrum is dominated by OH vibrations of water molecules that are located on the surface of the protein. The strong band at 3,200 cm^{-1} has a similar shape and central frequency as the OH vibration spectrum of ice, i.e., water below the freezing point (24–26). This band is, however, observed at the surface of AFP-III at room temperature. Control experiments using other proteins do not show this spectral response (Fig. S2). Hence, the strong peak at 3,200 cm^{-1} is specifically related to the AFP. We assign this band to the response of ice-like water layers associated with the IBS of the protein. To test the assignment of the strong peak at 3,200 cm^{-1} to ice-like water layers, we studied an inactive mutant of AFP-III. In the used mutant (T18N), the threonine 18 residue in the center of the IBS was replaced by asparagine which resulted in elimination of antifreeze activity (Fig. S3). In Fig. 3, we compare the VSFG spectrum of T18N with that of active AFP-III at different concentrations. The VSFG spectrum of T18N shows distinct features in the CH stretching region (2,880 cm^{-1}, 2,950 cm^{-1}) and a broad feature in the OH-stretching region. The most obvious difference between the spectra of active AFP-III and the inactive mutant T18N is the absence of the ice peak at 3,200 cm^{-1} in the spectrum of the mutant. Further differences can be seen in the intensities of the different CH signals. Altogether, the T18N spectrum is similar to the VSFG spectra of other (nonantifreeze) proteins and with the AFP-III spectra at low concentrations, where the VSFG spectrum is dominated by the electric field effect of proteins on the liquid water spectrum, and no longer represents the spectrum of water adsorbed to the protein surface. The VSFG spectrum of T18N shows that the loss of antifreeze activity directly correlates with the disappearance of the formation of ice-like water layers. This finding agrees well with the results of molecular simulations, demonstrating that the loss of antifreeze activity by a mutation in the IBS is associated with a disruption of the ice-like pattern of the hydrating water molecules (15). In Fig. 4, we show VSFG spectra of AFP-III solutions at different temperatures. Upon lowering the temperature, the ice peak increases in amplitude while the CH signals remain the same. This result shows that more ice-like water is involved when the temperature is decreased. The ice peak also shows a small red shift, which shows that the hydrogen bonding in the ice-like water layers is only slightly enhanced as the solution temperature is decreased toward the freezing point. No further spectral change is observed upon lowering the temperature below the freezing point: The spectra taken at 0 °C and −2.5 °C are almost identical in amplitude and shape. This

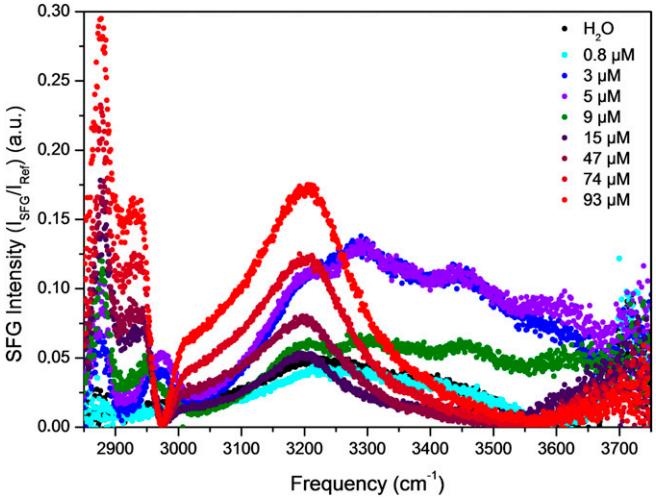

Fig. 2. VSFG spectra of the water–air interface and aqueous solutions of AFP-III of different concentration (0–90 μM). The VSFG spectra of AFP-III strongly depend on concentration. At concentrations below 10 μM (navy blue), the spectra are similar to the VSFG spectrum of water–air, except for the band at 3,600 cm^{-1} that can be assigned to water molecules that are weakly hydrogen-bonded to the protein. A similar response is observed for other proteins (see Fig. S2). For concentrations >10 μM, the broad response in the OH stretch region disappears and a relatively narrow peak at 3,200 cm^{-1} rises. This peak is assigned to water molecules contained in ice-like layers bound to the IBS of the AFP-III protein.

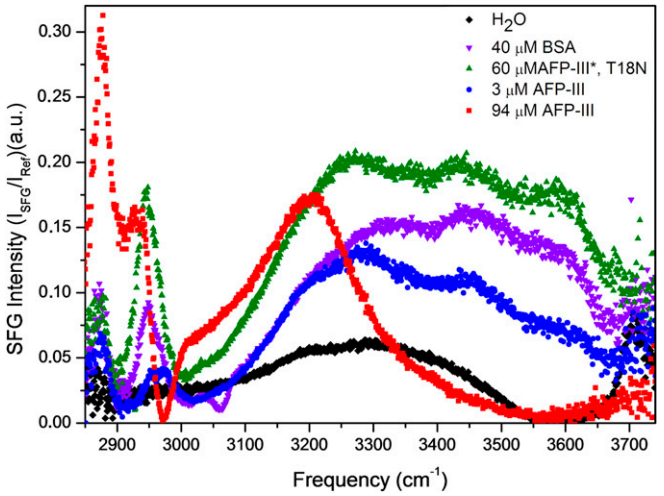

Fig. 3. VSFG spectra of active AFP-III and an inactive T18N AFP-III mutant at room temperature. The VSFG spectrum of the T18N mutant does not show the ice peak at 3,200 cm^{-1} that is observed for active AFP-III. The VSFG spectrum of the T18N mutant (green) shows two distinct features corresponding to CH vibrations and a broad response in the OH stretching region between 3,200 cm^{-1} and 3,600 cm^{-1}. The spectrum of the T18N mutant is similar to that of other (nonantifreeze) proteins (BSA, purple) and to that of AFP-III at low concentrations (blue), where the VSFG spectrum no longer represents the response of water bound to the protein surface but rather the effect of the local electric field of the protein on the response of the liquid water–air interface.

could point toward an optimization of the ice-like hydration layer close to the temperature at which AFPs function in polar fish blood. The signals in the CH region remain constant over the investigated temperature range, which indicates that the IBS of AFP-III does not show structural or conformational changes upon lowering the temperature.

Discussion

The presence of ordered water molecules at the surface of AFPs has been predicted by simulations (14, 15, 27–30), and ordered water molecules have been observed at the surfaces of different proteins (including non-AFP) using high-resolution X-ray crystallography (31, 32). For instance, in a recent X-ray diffraction study of a novel AFP, it was found that the protein contains more than 400 water molecules in its hydrophobic core. This core extends outward, and ordered water molecules are believed to form the adjacent IBS (32). All of the X-ray crystallographic studies were performed on protein crystals at temperatures far below the freezing point, typically at −196 Celsius, i.e., at highly nonphysiological conditions. Hence, from the X-ray studies, it is not clear whether ordered water molecules can also exist at protein surfaces exposed to liquid water at temperatures above the freezing point. The present results give clear proof of the existence of ice-like water layers on the surface of a protein under physiological conditions, i.e., embedded in liquid water and at temperatures above the freezing point.

A recent Raman study showed that the hydrophobic alkyl groups of alcohols enhance the hydrogen bonding and tetrahedral character of nearby water molecules (33) but not to the extent that we observe here for AFP-III. The rather pure ice-like character of the water layers bound to the IBS of AFP-III can be explained by the extended character of this surface, thus imposing the ice-like structure over a much larger length scale. Our results give evidence that biomolecules are able to fine-tune the structure of water to a specific function by using a subtle spatial arrangement of hydrophobic and allegedly hydrophilic side chain residues as illustrated by the presence of both hydrophobic and hydrophilic amino acids in the IBS of AFP-III (10). The results underline the need to include surrounding water molecules for the full understanding of biomolecular recognition and interaction.

The observation of ice-like water layers at the surface of AFPs at temperatures well above the freezing point is a key finding in understanding the details of the adsorption–inhibition mechanism of antifreeze activity at the molecular level. Thereby our results strongly support the preordering–binding (POB) mechanism for the recognition and the subsequent attachment to ice, as initially proposed by Nutt and Smith (28). The preordered ice-like water domains will have an affinity and specificity for similar ice-like water and therefore for ice itself. We hypothesize that upon binding of AFP-III with its ice-like hydration layer to the correct surface plane of a growing ice crystal, the ice-like layers merge with the ice crystal. Consequently, the actual binding would occur via a mostly enthalpic interaction between the preordered ice-like hydration layer of the protein and the OH groups of the nascent ice front.

Materials and Methods

SFG Experiments. The laser source for the SFG setup is a regenerative Ti:Sapphire amplifier (Coherent) producing 800-nm pulses at a 1-kHz repetition rate with a pulse duration of 35 fs and a pulse energy of 3.5 mJ. Approximately one third of the laser output is used to pump a home-built optical parametric amplifier and a difference frequency mixing stage. This nonlinear optical device produces tunable broadband mid-IR pulses (ranging from 2 μm to 10 μm, 600 cm_{-}^{1} bandwidth at FWHM, 10–20 μJ). The IR pulses have a sufficiently large bandwidth to measure the complete SFG spectrum of the OH (OD) stretch vibrations of H_2O (D_2O). Another part of the 800-nm pulse is sent through an etalon to narrow down its bandwidth to ∼15 cm^{-1}. The resulting narrow-band 800-nm pulse (VIS) and the broadband IR pulse are directed to the sample surface at angles of ∼50° and ∼55°, respectively, to generate light at the sum frequency. The VIS and IR beams are focused in spatial and temporal overlap on the sample surface with 200-mm and 100-mm focal length lenses, respectively. The SFG light generated at the surface is sent to a monochromator and detected with an Electron-Multiplied Charge Coupled Device (EMCCD, Andor Technologies). All spectra in this paper were recorded with s-polarized SFG, s-polarized VIS, and p-polarized IR (with respect to the plane of incidence). The spectra are first background subtracted (blocked IR) and normalized to a reference SFG spectrum measured from z-cut quartz. As a measurement cell, we used a temperature-controlled Teflon-coated aluminum cell with a CaF_2 window on top as

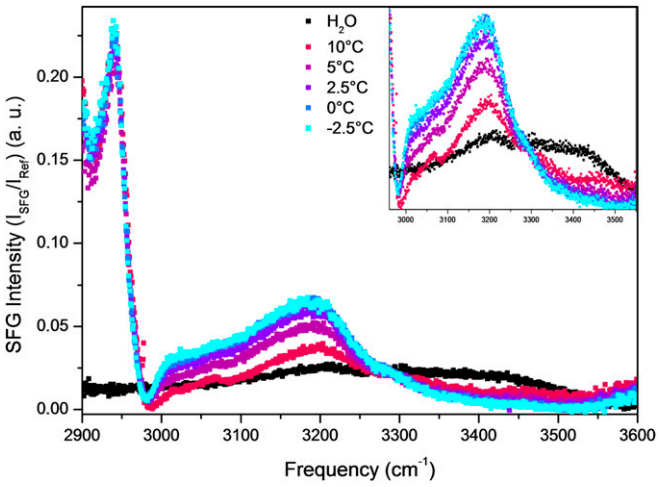

Fig. 4. VSFG spectra of a 20-μM AFP-III (pH 7.8) at different temperatures. For comparison, the VSFG of the water–air interface is also shown (black). Decreasing the temperature leads to an increase and a small redshift of the band at 3,200 cm^{-1}. The CH signals show no change upon lowering the temperature, indicating that the protein conformation is conserved in the studied temperature range. *Inset* shows a zoom in of the spectral region between 2,950 cm^{-1} and 3,550 cm^{-1}.

shown in Fig. S4. The temperature of the cell can be varied using a Peltier element. Purity is an important issue when performing SFG experiments on AFPs. Impurities such as salts, organic contaminations, or inactive isoforms can lead to competitive adsorption on the water–air interface and can lead to false results (16). Therefore, measurements were performed in pure water (Milipore), and only AFP-III samples with known antifreeze activity and high purity were used. The surface tension (Kibron Inc., Wilhelmy plate method) and the pH (Mettler Toledo FE20) were checked before and after the SFG measurements for every sample.

AFPs. AFP-III is a 7-kDa globular protein that can be found in both Arctic and Antarctic fish (34). Type AFP-III was extensively investigated using various theoretical and experimental methods (10–15). These studies identified the region of the protein that is responsible for the binding to ice to be hydrophobic and rather flat. Several site-directed mutagenesis studies further explored the IBS of the protein and identified 11 amino acids that were crucial for activity (10, 35–37). Fig. S1 shows the IBS of AFP-III including the labeled residues mandatory for activity. Among different fish, the protein can slightly differ in size but shows a remarkably high amino acid sequence identity. It is therefore assumed that the IBS of different AFP-IIIs is very similar, as indicated by a direct comparison by Howard et al. (11). Within our studies, we investigated both AFP-III purified from the blood of Antarctic fish and AFP-III proteins obtained by recombinant protein expression, including a mutant T18N AFP-III. In this mutant the threonine residue at position 18 is replaced by asparagine. Thr18 has a central position in the IBS that binds AFP-III to the primary prism plain of ice (10). Since the 3D structure (PDB File 1JAB) (37) and hydrophobicity of the T18N mutant is highly similar to that of wild-type AFP-III (PDB file 1HG7) (38), the observed changes in the SFG spectrum cannot be explained by a different orientation or propensity at the interface.

Recombinant Expression and Purification of Type III AFP. The gene encoding for AFP-III from ocean pout (rQAE isoform, M1.1HISPET20b) (31) was kindly provided by Peter Davies (Queen's University, Kingston, Canada). The cDNA was inserted in between the Nde1/Xho1 restriction sites of the pET20b expression vector (Novagen) in frame with the His-tag sequence. The plasmid was transformed into competent *Escherichia coli* NiCo21(DE3) cells (New England Biolabs). Positive clones were selected and incubated overnight at 37 °C under continuous shaking at 250 rpm in a 25-mL preculture of LB-medium with 100 μg/mL ampicillin and 0.5% glucose. The preculture was transferred to a 5-L culture flask and cells were grown in 1 L of ZYP-5052 autoinduction medium containing 100 μg/mL ampicillin at 37 °C under continuous shaking at 130 rpm (39). The temperature of the culture was reduced to 18 °C when the OD_{600nm} reached 2–2.5, and overexpression of the protein was allowed overnight under shaking. Successful overexpression of the target protein was confirmed by SDS/PAGE. Cells were pelleted by centrifugation and lysed using BugBuster (Novagen) via 40 min shaking at room temperature. The cell lysate was spun down and the supernatant applied to a Ni-NTA agarose (Novagen) column equilibrated with bind buffer (20 mM Tris pH 8, 150 mM NaCl, 5 mM imidazole). The column was washed with four to five column volumes of wash buffer (20 mM Tris pH 8, 150 mM NaCl, 30 mM imidazole), and the protein was eluted with 400 mM imidazole. The fractions containing rQAE and T18N were collected and dialyzed overnight against 20 mM Tris pH 7.5 using 1-kDa dialysis membranes (Spectra/Por 6) and concentrated using 3-kDa Microsep Advance centrifugal devices (Pall). Purity was estimated by SDS/PAGE gel electrophoresis and the exact mass determined using Quadrupole Time of Flight (Q-ToF) mass spectroscopy. The protein concentration was determined by UV absorbance using the molar extinction coefficient $\varepsilon_{280} = 1{,}568\ M^{-1}{\cdot}cm^{-1}$ as reported in literature (39). Typical yields per liter of culture medium were ∼80 mg.

Characterization of AFP-III by Q-ToF Mass Spectrometry and Sonocrystallization. ***Q-ToF mass spectrometry.*** The purity and exact mass of the recombinantly expressed protein samples were assessed on a Waters Xevo G2 Q-ToF liquid chromatography-mass spectrometry system equipped with an Agilent Polaris C18A RP column. Samples were measured at approximate concentration of 0.1 mg/mL. The MaxENT algorithm was used to deconvolute the mass spectra.
Sonocrystallization. The sonocrystallization setup was built according to the original design by Grunwald and coworkers (40). The temperature-controlled sample chamber consists of a heating unit positioned inside an aluminum cooling block, which is cooled using an external cooling bath (Julabo CF40) with 50/50 ethanol/water as coolant to −15 °C. The heating unit consists of a copper coil wrapped around a copper tube. The temperature is controlled by applying energy to the heating wire via an adjustable power supply unit. The sample is loaded in a 2-mL Eppendorf and inserted into the copper tube. A coated stirring bar was inserted to ensure a homogenous temperature through the whole sample (sample volume ∼0.8–1 mL). Two Pt-100 resistance thermometers (JUMO; PG 1.0910.1) are used in the setup, one inserted into the heating unit (T1) used to control the temperature of the chamber, and the other inserted into the sample tube (T2) to monitor the heating profile of the sample. Ice crystallization is initiated by the application of a short ultrasound pulse (100 ms, 30% amplitude) via the sonotrode (Sonics; VCX 130PB) inserted 0.5 cm deep into the sample.

The temperature sensor (T2) inserted into the sample was calibrated using an osmolality linearity set (Advanced Instruments) with five solution concentrations (0, 100, 250, 500, and 750 $mOsm{\cdot}kg^{-1}$) such that the difference between the calculated and measured freezing point of the solutions was within 0.02 °C. The temperature sensor of the heating unit (T1) was adjusted accordingly. Freezing hysteresis is determined from the T2 values determined at the two plateaus that develop upon setting T1 to −6 °C and 0.4 °C in a temperature ramp consisting of six steps. The starting temperature of each ramp is 10 °C (step 1), after which T1 is reduced to −6 °C at a rate of 1.5 °C min^{-1} (step 2). A short ultrasound pulse is hereafter applied and the temperature is kept at 6 °C for 300 s (step 3), after which T1 is raised to 0.4 °C at a rate of 1.5 °C min^{-1} (step 4) and kept constant at 0.4 °C for 650 s (step 5). Finally, T1 is further increased to the initial temperature of 10 °C (step 6). Throughout the temperature ramp, data are recorded using a home-written LabView program.

ACKNOWLEDGMENTS. This work is part of the research program of the Stichting voor Fundamenteel Onderzoek der Materie, which is financially supported by the Nederlandse Organisatie voor Wetenschappelijk Onderzoek (NWO). I.K.V. is grateful for financial support from NWO (Veni Grant 700.10.406) and the European Union (FP7-PEOPLE-2011-CIG Contract 293788 and FP7-PEOPLE-2012-ITN Contract 316866).

1. Ball P (2008) Water as an active constituent in cell biology. *Chem Rev* 108(1):74–108.
2. Zhong D, Pal SK, Zhang D, Chan SI, Zewail AH (2002) Femtosecond dynamics of rubredoxin: Tryptophan solvation and resonance energy transfer in the protein. *Proc Natl Acad Sci USA* 99(1):13–18.
3. Grossman M, et al. (2011) Correlated structural kinetics and retarded solvent dynamics at the metalloprotease active site. *Nat Struct Mol Biol* 18(10):1102–1108.
4. Chong S-H, Ham S (2014) Interaction with the surrounding water plays a key role in determining the aggregation propensity of proteins. *Angew Chem Int Ed Engl* 53(15):3961–3964.
5. Prabhu N, Sharp K (2006) Protein-solvent interactions. *Chem Rev* 106(5):1616–1623.
6. Duman JG (2001) Antifreeze and ice nucleator proteins in terrestrial arthropods. *Annu Rev Physiol* 63:327–357.
7. Yeh Y, Feeney RE (1996) Antifreeze proteins: Structures and mechanisms of function. *Chem Rev* 96(2):601–618.
8. DeVries AL (1971) Glycoproteins as biological antifreeze agents in Antarctic fishes. *Science* 172(3988):1152–1155.
9. Raymond JA, DeVries AL (1977) Adsorption inhibition as a mechanism of freezing resistance in polar fishes. *Proc Natl Acad Sci USA* 74(6):2589–2593.
10. Garnham CP, et al. (2010) Compound ice-binding site of an antifreeze protein revealed by mutagenesis and fluorescent tagging. *Biochemistry* 49(42):9063–9071.
11. Howard EI, et al. (2011) Neutron structure of type-III antifreeze protein allows the reconstruction of AFP-ice interface. *J Mol Recognit* 24(4):724–732.
12. Siemer AB, Huang KY, McDermott AE (2010) Protein–ice interaction of an antifreeze protein observed with solid-state NMR. *Proc Natl Acad Sci USA* 107(41):17580–17585.
13. Baardsnes J, Davies PL (2002) Contribution of hydrophobic residues to ice binding by fish type III antifreeze protein. *Biochim Biophys Acta* 1601(1):49–54.
14. Gallagher KR, Sharp KA (2003) Analysis of thermal hysteresis protein hydration using the random network model. *Biophys Chem* 105(2-3):195–209.
15. Yang C, Sharp KA (2004) The mechanism of the type III antifreeze protein action: A computational study. *Biophys Chem* 109(1):137–148.
16. Engelhardt K, Peukert W, Braunschweig B (2014) Vibrational sum-frequency generation at protein modified air–water interfaces: Effects of molecular structure and surface charging. *Curr Opin Colloid Interface Sci* 19(3):207–215.
17. Shen YR, Ostroverkhov V (2006) Sum-frequency vibrational spectroscopy on water interfaces: Polar orientation of water molecules at interfaces. *Chem Rev* 106(4):1140–1154.
18. Mondal JA, Nihonyanagi S, Yamaguchi S, Tahara T (2010) Structure and orientation of water at charged lipid monolayer/water interfaces probed by heterodyne-detected vibrational sum frequency generation spectroscopy. *J Am Chem Soc* 132(31):10656–10657.
19. Nihonyanagi S, Yamaguchi S, Tahara T (2010) Water hydrogen bond structure near highly charged interfaces is not like ice. *J Am Chem Soc* 132(20):6867–6869.
20. Salvay AG, et al. (2010) Structure and interactions of fish type III antifreeze protein in solution. *Biophys J* 99(2):609–618.
21. Du Q, Superfine R, Freysz E, Shen YR (1993) Vibrational spectroscopy of water at the vapor/water interface. *Phys Rev Lett* 70(15):2313–2316.

22. Sovago M, et al. (2008) Vibrational response of hydrogen-bonded interfacial water is dominated by intramolecular coupling. *Phys Rev Lett* 100(17):173901.
23. Pieniazek PA, Tainter CJ, Skinner JL (2011) Interpretation of the water surface vibrational sum-frequency spectrum. *J Chem Phys* 135(4):044701.
24. Anim-Danso E, Zhang Y, Alizadeh A, Dhinojwala A (2013) Freezing of water next to solid surfaces probed by infrared-visible sum frequency generation spectroscopy. *J Am Chem Soc* 135(7):2734–2740.
25. Bisson PJ, Shultz MJ (2013) Hydrogen bonding in the prism face of ice I(h) via sum frequency vibrational spectroscopy. *J Phys Chem A* 117(29):6116–6125.
26. Barnett IL, Groenzin H, Shultz MJ (2011) Hydrogen bonding in the hexagonal ice surface. *J Phys Chem A* 115(23):6039–6045.
27. Meister K, et al. (2013) Long-range protein–water dynamics in hyperactive insect antifreeze proteins. *Proc Natl Acad Sci USA* 110(5):1617–1622.
28. Nutt DR, Smith JC (2008) Dual function of the hydration layer around an antifreeze protein revealed by atomistic molecular dynamics simulations. *J Am Chem Soc* 130(39):13066–13073.
29. Smolin N, Daggett V (2008) Formation of ice-like water structure on the surface of an antifreeze protein. *J Phys Chem B* 112(19):6193–6202.
30. Midya US, Bandyopadhyay S (2014) Hydration behavior at the ice-binding surface of the *Tenebrio molitor* antifreeze protein. *J Phys Chem B* 118(18):4743–4752.
31. Garnham CP, Campbell RL, Davies PL (2011) Anchored clathrate waters bind antifreeze proteins to ice. *Proc Natl Acad Sci USA* 108(18):7363–7367.
32. Sun T, Lin FH, Campbell RL, Allingham JS, Davies PL (2014) An antifreeze protein folds with an interior network of more than 400 semi-clathrate waters. *Science* 343(6172):795–798.
33. Davis JG, Gierszal KP, Wang P, Ben-Amotz D (2012) Water structural transformation at molecular hydrophobic interfaces. *Nature* 491(7425):582–585.
34. Schrag JD, Cheng CH, Panico M, Morris HR, DeVries AL (1987) Primary and secondary structure of antifreeze peptides from arctic and antarctic zoarcid fishes. *Biochim Biophys Acta* 915(3):357–370.
35. Chao H, Sönnichsen FD, DeLuca CI, Sykes BD, Davies PL (1994) Structure-function relationship in the globular type III antifreeze protein: Identification of a cluster of surface residues required for binding to ice. *Protein Sci* 3(10):1760–1769.
36. DeLuca CI, Davies PL, Ye Q, Jia Z (1998) The effects of steric mutations on the structure of type III antifreeze protein and its interaction with ice. *J Mol Biol* 275(3):515–525.
37. Graether SP, et al. (1999) Quantitative and qualitative analysis of type III antifreeze protein structure and function. *J Biol Chem* 274(17):11842–11847.
38. Antson AA, et al. (2001) Understanding the mechanism of ice binding by type III antifreeze proteins. *J Mol Biol* 305(4):875–889.
39. Studier FW (2005) Protein production by auto-induction in high density shaking cultures. *Protein Expr Purif* 41(1):207–234.
40. Gaede-Koehler A, Kreider A, Canfield P, Kleemeier M, Grunwald I (2012) Direct measurement of the thermal hysteresis of antifreeze proteins (AFPs) using sonocrystallization. *Anal Chem* 84(23):10229–10235.

Supporting Information

Meister et al. 10.1073/pnas.1414188111

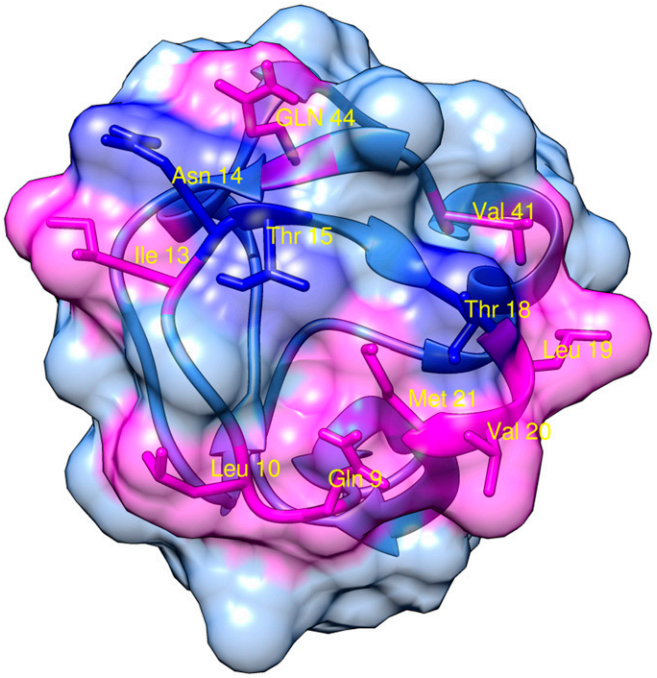

Fig. S1. Top view of the IBS of AFP-III. Amino acids that have previously been reported to be mandatory for activity are highlighted and labeled. The hydrophobic residues are shown in magenta and the hydrophilic residues in dark blue.

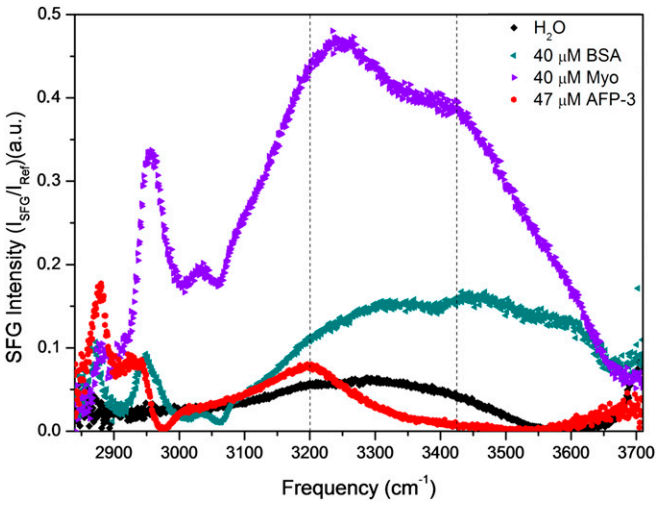

Fig. S2. VSFG spectra of AFP-III and nonantifreeze proteins. For all investigated nonantifreeze protein solutions the VSFG spectrum of the water OH stretch vibrations strongly differs from the VSFG spectrum of water at the surface of AFP-III. Non-AFP proteins (BSA, pH 7.5; Myoglobin, pH 7.1) show a very broad structured response in the OH region ranging from 3,200 cm^{-1} to 3,600 cm^{-1}, with strong similarity to the VSFG spectrum of the liquid water–air interface. Only AFP-III (blue) shows a single relatively narrow feature at 3,200 cm^{-1}, which we assign to ice-like water layers at the surface of the protein.

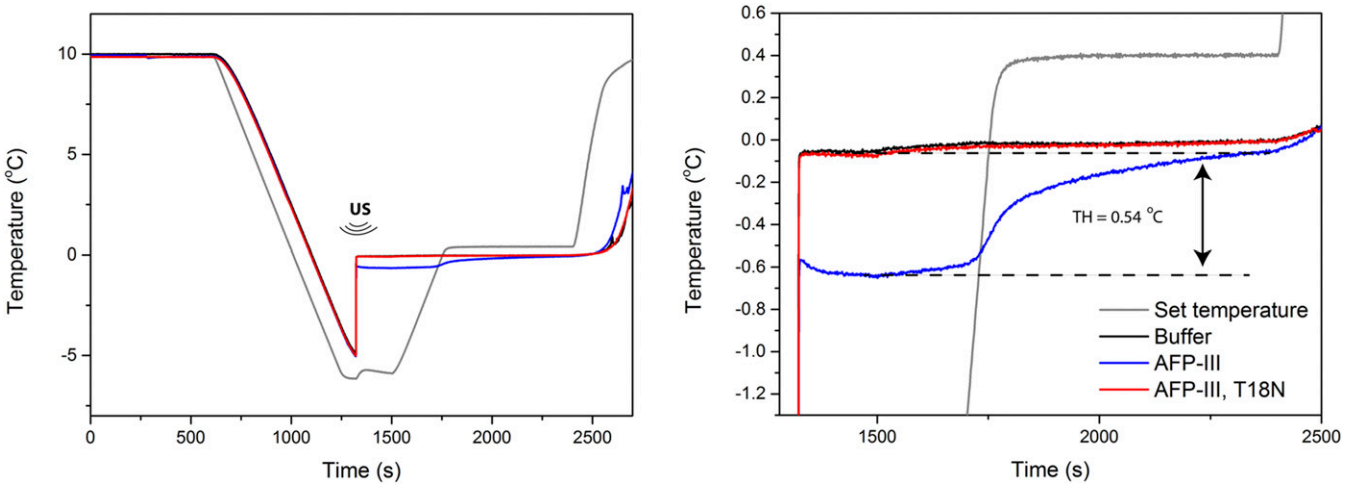

Fig. S3. Comparison of the antifreeze activity of AFP-III and the mutant T18N by sonocrystallization. Thermal hysteresis activity of 3 mg/mL solutions of AFP-III and the T18N mutant in 20 mM Tris pH 7.5 have been determined by sonocrystallization through the application of a well-defined temperature ramp as indicated by the gray line. A short ultrasound pulse (100 ms) is applied when the temperature is set to −6 °C to initiate ice crystallization, which subsequently releases latent heat until the sample temperature reaches the nonequilibrium freezing point. Hereafter the sample temperature is then slowly raised to 0.4 °C to determine the melting point. This allows for an accurate determination of thermal hysteresis (TH), defined as the difference between the melting and freezing point. For wild-type AFP-III, we determine TH = 0.54 °C by sonocrystallization, which is in close agreement with the TH = 0.58 °C by nanoliter osmometry determined previously by others (1). By contrast, the temperature profile of the T18N mutant is identical to that of the 20 mM Tris pH 7.5 buffer, which demonstrates that a single-point mutation can completely eliminate thermal hysteresis activity. Note that a reduction of 10% in activity has previously been reported for T18N as determined by nanolitre osmometry by others (2).

1. Baardsnes J, Davies PL (2002) Contribution of hydrophobic residues to ice binding by fish type III antifreeze protein. *Biochim Biophys Acta* 1601(1):49–54.
2. Graether SP, et al. (1999) Quantitative and qualitative analysis of type III antifreeze protein structure and function. *J Biol Chem* 274(17):11842–11847.

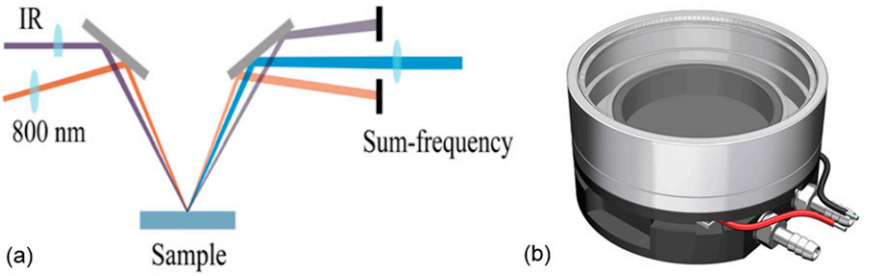

Fig. S4. Schematic Illustrations of the SFG setup (*A*) and the temperature-controlled measurement cell (*B*).

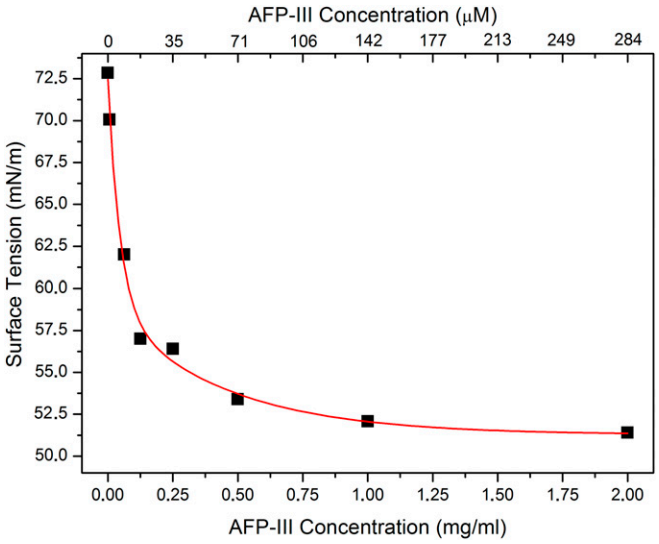

Fig. S5. Surface tension as a function of concentration of AFP-III. The red line is a guide to the eye. The effect of AFP-III on the surface tension becomes significant for concentrations >10 μM and starts to saturate for concentrations >100 μM. These observations agree with the SFG spectral data of Fig. 2. Our surface tension values agree qualitatively with results obtained by Salvay et al. (1). Their lower values are probably due to differences in stirring time, initial solution temperature, or origin and purity of the AFP.

1. Salvay AG, et al. (2010) Structure and interactions of fish type III antifreeze protein in solution. *Biophys J* 99(2):609–618.